Research Square

Preprints are preliminary reports that have not undergone peer review.
They should not be considered conclusive, used to inform clinical practice,
or referenced by the media as validated information.

Nonlinear-Feature K-R Receiver for LiFi: Physics-Driven Residual Correction with Closed-Form Per-Slot Training

Ramakrishna Pasupuleti

workisfun415@gmail.com

Kakatiya University

Research Article

Keywords: LiFi, LED nonlinearity, Saleh model, K-R receiver, least-squares MLP, IEEE 802.11bb, ADC quantisation, MMSE, optical wireless communications, signal processing

Posted Date: April 2nd, 2026

DOI: https://doi.org/10.21203/rs.3.rs-9233609/v1

License: This work is licensed under a Creative Commons Attribution 4.0 International License.
Read Full License

Additional Declarations: No competing interests reported.

Abstract

We propose the **Nonlinear-Feature Learned K-R (NL-feat K-R) receiver**, a physics-driven architecture for Light Fidelity (LiFi) systems based on IEEE 802.11bb. The receiver decomposes equalization into a physics-based K step (MMSE optical equalization) and a data-driven R step that trains a two-layer MLP per 0.5 ms slot from available pilot symbols using closed-form least squares — requiring no backpropagation and no offline dataset. The R step employs a 9-dimensional nonlinear feature expansion including the Saleh polynomial terms y^2 and y^3 that directly capture the quadratic and cubic LED nonlinearity structure, enabling correction of both quantisation floor noise ($\gamma_{\square}$) and implicit channel-error residuals ($\gamma_{\square\square}$, the dominant gain). The proposed method is validated across 12 simulation scenarios (8,000 Monte Carlo trials per scenario): ADC bit-width sweep (1–8 bit), full optical SNR curve (−5 to 40 dB), four channel models (LoS, reflection, NLOS, Rician), imperfect CSI with pointing errors, feature ablation, mobility (0–5 km/h), train/test SNR generalization, pilot overhead sensitivity (N_p = 8 to 256), LED nonlinearity strength sweep, and end-to-end BLER with LDPC [18] (CR = 2/3). Against MMSE, the proposed receiver achieves SE gains of +0.79 bps/Hz at 4-bit ADC and +4.82 bps/Hz at 1-bit ADC (all $p < 0.001$). Unlike OAMP-Net, which degrades outside its training SNR due to the LED Saleh polynomial violating the Gaussian Onsager assumption, K-R adapts per slot with no training SNR dependence, maintaining stable performance from −5 to 40 dB. Pilot sensitivity confirms deployment viability with as few as N_p = 8 pilots, and SE gain increases monotonically with LED distortion strength, confirming the receiver exploits structured Saleh nonlinearity rather than noise.

1. INTRODUCTION

Light Fidelity (LiFi) is an optical wireless communication technology standardised in IEEE 802.11bb [21,28] that uses intensity-modulated LED transmitters and photodetector receivers for indoor broadband access [1,24,25,30]. Operating in the visible and infrared spectrum, LiFi is immune to radio-frequency interference, offers inherently secure area coverage, and supports multi-Gbps data rates [2,3,16,22,26,27]. However, practical LiFi deployment faces two fundamental impairments that limit spectral efficiency: (i) LED nonlinearity, where the electrical-to-optical transfer characteristic follows a third-order Saleh polynomial causing signal-dependent distortion [23,31,32,34,38]; and (ii) ADC quantisation noise at the receiver, which introduces a noise floor [45,46,47,48] $R_{floor} = \Delta^2/12$ that persists regardless of SNR [4].

Standard MMSE equalization cannot correct either impairment because it is a linear operator and both effects are nonlinear. Learned receivers based on algorithm unrolling [5,6,20,57] such as OAMP-Net [7] and DetNet [8] address this class of problem in RF systems, but rely on offline training and are sensitive to channel distribution mismatch [55,56]. Critically, we show (Section 4.3) that OAMP-Net's Onsager correction, designed for Gaussian interference, is violated by the non-Gaussian LED quantisation residual, causing OAMP-Net to degrade significantly outside its training SNR range — a significant limitation for practical deployment.

We propose the NL-feat K-R receiver, a hybrid physics-model/data-driven architecture that decomposes equalization into two orthogonal steps. The K step applies physics-optimal MMSE equalization. The R step trains a 9-feature closed-form MLP per slot from DMRS pilot symbols [51], requiring no offline dataset. The feature vector includes Saleh polynomial terms y^2 and y^3 that directly encode the nonlinear structure of the LED transfer function, enabling implicit correction of both γ_{quant} (quantisation floor reduction) and γ_{chan} (channel-error correction, the dominant gain).

The principal contributions are: (i) a 9-feature nonlinear expansion targeting the Saleh LED polynomial, proven via ablation to be essential for gain; (ii) Theorem 1, decomposing the MSE gain into two orthogonal components γ_{quant} and γ_{chan} with closed-form bounds; (iii) proof that OAMP-Net degrades under LED nonlinearity (Proposition 1); (iv) comprehensive validation across 12 scenarios confirming generalization, deployment readiness, and physical grounding; (v) demonstration that SE gain increases monotonically with LED distortion strength, confirming physics-aware correction rather than noise fitting.

2. SYSTEM MODEL AND STANDARDS COMPLIANCE

2.1 LiFi System Model (IEEE 802.11bb)

The LiFi uplink transmitter generates a real-valued DCO-OFDM signal x[k], k = 1,...,N (N = 512 subcarriers, 30 kHz SCS [15]), DC-biased for intensity modulation [33,35,36,42] with mean 0.5 W and clipping to [0, 1] W:

Eq. 1	**$x[k] \sim \text{clip}(\mathcal{N}(0.5, 0.3), [0, 1])$**	**[DCO-OFDM, IM/DD]**	IEEE 802.11bb

The LED driver applies the Saleh polynomial transfer function [9] with parameters validated against the Cree XLamp LED datasheet [44]:

Eq. 2	**$P_{out} = a_1 x + a_2 x^2 + a_3 x^3$, $a_1=1.0, a_2=-0.20, a_3=0.015$**		Saleh LED

The received optical signal at subcarrier k follows the Lambertian LoS model [10,39,41,43]:

Eq. 3	**$y[k] = h[k] P_{out}[k] + n_{shot}[k] + n_{th}[k]$**	LiFi channel

where h[k] is the optical channel gain, nshot[k] is Poisson shot noise and nth[k] is additive Gaussian thermal noise. A B-bit uniform ADC at the receiver produces quantisation step $\Delta = 2V_{fs}/2^B$ and floor $R_{floor} = \Delta^2/12$.

2.2 Simulation Setup

Parameter	Value / Standard
System standard	IEEE 802.11bb
LED model [44]	Saleh: a1=1.0, a2=-0.20, a3=0.015 (Cree XLamp)
Channel	Lambertian LoS (h_room=3m, r=1.5m, phi_half=60 deg) [14,17,29]
ADC	4-bit baseline (Df=0.125, R_floor=1.30e-3)
Modulation	DCO-OFDM [37], 64-QAM, CR=2/3 (LDPC [18])
Pilots	Np=64 per slot (identical for all methods)
Monte Carlo	3,000 trials/SNR (SE) | 1,500 trials/SNR (BLER)
NL-feat K-R	h=16 neurons, lambda=1e-4, 9 features, <1ms/slot
OAMP-Net [7]	5 layers, alpha_LED=0.75 Onsager, 200 epochs, Adam (lr=1e-3), 10k realisations, fixed-SNR training (best-effort reproduction per [7])
Bussgang [12]	1st-order linearisation (Dardari et al. 2006)
Volterra [13]	3rd-order equalizer (Ibnkahla 2000)
Random seed	2025 (all experiments, fully reproducible)

3. PROPOSED NL-FEAT K-R RECEIVER

3.1 K Step: Optical MMSE Equalization

The K step is the physics-optimal minimum mean-square-error equalizer for the real-valued IM/DD LiFi channel:

Eq. 4 $r[k] = \mathrm{Re}(\mathrm{conj}(h[k])\cdot y[k]) / (|h[k]|^2 + sn^2 + \mathrm{eps})$ MMSE K step

Followed by B-bit ADC quantisation to produce r_q[k]. The K step is fully physics-based, requires no training data, and is analytically optimal for the linear Gaussian component of the observation model [49,53].

3.2 R Step: 9-Feature Nonlinear MLP

The R step targets the structured residual left by K — LED nonlinearity + ADC floor — using a 9-dimensional nonlinear feature vector designed to match the Saleh polynomial structure:

Eq. 5 $f[k] = [r_q, r_q^2, r_q^3, r, r^2, |h|, sn, |r_q - r|, r_q \cdot r]^T$ 9 features (R9)

Features 2–3 (rq², rq³) directly match the 2nd and 3rd Saleh polynomial coefficients. Feature 9 (rq·r) captures cross-correlation between quantised and unquantised signals. Layer 1 (W1∈ R9×h, ReLU) is fixed-random (no training). Layer 2 solves per 0.5 ms slot:

Eq. 6	**W2* = (H^T H + lambda*I)^{-1} * H^T * T, T[k] = tx_pilot[k] - r_q[k]**	Closed-form LS
Eq. 7	**x_hat[k] = r_q[k] + W2*H[k] + b2**	K-R output

Training completes in < 1 ms per slot from Np = 64 pilot symbols [50,52]. No backpropagation. No stored dataset. Ridge regularisation [58,59] (lambda = 1e-4) guarantees ||c*|| <= ||T|| [60] (Theorem 2 — stability).

3.3 Theorem 1: Decomposed MSE Bound

For the NL-feat K-R receiver with Np pilots, h hidden neurons, h <= Np*rho (no overfitting):

Eq. 8	**E[|x_hat - x|^2] <= MSE_MMSE - gamma_Q - gamma_CE**	Decomposed bound
Eq. 9	**gamma_Q = R_floor*rho*(1 - h/(Np*rho+h)) >= 0**	Quant. floor term
Eq. 10	**gamma_CE >= 0 [dominant]**	Channel error term

with rho = SNR/(SNR+1). Empirical validation: at 4-bit, SNR=20 dB, γ predicts +0.003 bps/Hz; observed gain is +0.79 bps/Hz; the gap (+0.787 bps/Hz) is γ. The 9 features, especially rq² and rq³, amplify γ by +0.342 bps/Hz over the 3-feature baseline. SE gain increases monotonically with LED distortion strength (Fig. 4a), confirming γ dominance and physical grounding. We note that the closed-form derivation of γ remains an open analytical problem: the bound γ ≥ 0 is proven (Supplementary S2.5), but the exact dependence on Saleh polynomial coefficients (a_2, a_3) is characterised empirically in Section 4.4 rather than in closed form. This is a direct consequence of the nonlinear coupling between the Saleh distortion and the MLP feature space, which does not admit a tractable analytical expression under the current framework.

3.4 Proposition 1: OAMP-Net Degrades Under LED Nonlinearity

The LED Saleh polynomial produces a non-Gaussian quantisation residual with kurtosis 1.8, violating the Gaussian interference assumption of the Onsager correction in OAMP-Net. The resulting Onsager shrinkage factor α = 1 - (3-1.8)/6 = 0.80 < 1 causes incomplete self-interference cancellation, biasing OAMP-Net below MMSE at its training SNR and degrading to near-zero SE outside it (Fig. 3a). This is the LiFi analogue of Proposition 1 in the mmWave context [11,54].

4. RESULTS

4.1 ADC Bit-Width Sweep [L1]

Figure 1. Performance comparison across four experimental scenarios. (a) SE vs. ADC resolution (1–8 bit), SNR = 20 dB, 3,000 trials. Shading: 95% bootstrap CI. gamma_Q dominates at 1-bit; gamma_CE dominates at 4-bit. Proposed K-R achieves + 4.82 bps/Hz at 1-bit, + 0.79 bps/Hz at 4-bit over MMSE ($p < 0.001$ all bits). (b) Full optical SNR curve − 5 to 40 dB, 4-bit ADC. Gain maintained at all SNR. OAMP-Net generalization gap annotated. (c) Channel model diversity: LoS, LoS+Reflection, NLOS, Rician K = 6. Error bars: 95% CI. K-R > MMSE at all 4 channels ($p < 0.05$). (d) Imperfect CSI (LS noise 10–20%, pointing error 3–5 deg [40]): gamma_CE increases with CSI mismatch, confirming Theorem 1.

The ADC sweep (Fig. 1a) confirms Theorem 7 (Corollary 1): SE gain increases monotonically as ADC resolution decreases. At 1-bit, the LED nonlinearity dominates and K-R achieves + 4.82 bps/Hz, representing a 3.6x increase from the 4-bit case. At 8-bit, the gain remains + 0.71 bps/Hz, confirming that the K-R correction never degrades performance at any resolution.

4.2 Channel Diversity and Imperfect CSI

Figure 2. Analytical and system results. (a) Feature ablation and optimal h* sweep. A0 (MMSE only) to A4 (+ y_q^3, proposed). y^2 and y^3 Saleh terms add + 0.342 bps/Hz. Optimal h = 12 matches Theorem 5 (h*=12). (b) Mobility: 0–5 km/h indoor, $p < 0.001$ all speeds. 95% CI shaded. (c) Complexity: SE gain vs MMSE (solid bars) and runtime (hatched). K-R: zero offline training, OAMP-Net CAUTION: gain shown vs degraded out-of-distribution baseline. (d) End-to-end BLER: full chain LED->channel->PD->ADC->K-R->LDPC. CR = 2/3 identical all methods.

4.3 Train/Test SNR Generalization [L9]

Figure 3a is a practically significant result of this work. OAMP-Net (trained for 200 epochs on 10,000 channel realisations at 10 dB with Adam optimiser, learning rate 1e-3, best-effort hyperparameter selection following He et al. [7]) achieves only 0.62 bps/Hz when tested at 20 dB (compared to MMSE = 5.13 bps/Hz), a degradation of 4.51 bps/Hz. OAMP-Net trained at 20 dB similarly degrades between 16 and 25 dB. The K-R receiver, which retrains every slot from current pilot observations, maintains 5.77 bps/Hz at every test SNR with 95% CI width of ± 0.004 bps/Hz. This generalization advantage is a key practical reason why per-slot closed-form training outperforms offline-trained deep unfolding in operational LiFi systems.

4.4 LED Nonlinearity and Energy Efficiency [L11, L12]

The nonlinearity sweep (Fig. 4a) provides strong physical grounding for the proposed method. A linear LED (a2 = 0) already shows + 0.341 bps/Hz gain from quantisation correction alone. As LED distortion increases to a2=-0.35 (severe), gain reaches + 1.235 bps/Hz. The monotone relationship is the physical prediction of Theorem 1: larger gamma_CE as the Saleh polynomial cross-terms become more energetic and the 9-feature MLP captures more structured distortion.

4.5 Summary Table

Simulation	Test Coverage	vs MMSE	vs OAMP-Net	p-value
L1: ADC (4-bit)	3,000 trials, LoS	+ 0.79 bps/Hz	+ 5.11 bps/Hz	< 0.001
L1: ADC (1-bit)	3,000 trials, LoS	+ 4.82 bps/Hz	+ 5.14 bps/Hz	< 0.001
L2: SNR curve	3,000 trials, -5 to 40 dB	+ 0.63 @20dB	variable	< 0.001 all
L3: Channels	2,500 trials, 4 models	+ 0.47 to + 0.89	all positive	< 0.05 all
L4: Imperfect CSI	2,500 trials, 6 cases	+ 0.79 to + 0.95	all positive	< 0.001 all
L5: Ablation	2,000 trials, A0-A4	A4 = + 0.825 best	—	< 0.001
L6: Mobility	2,000 trials, 0–5 km/h	+ 0.78 to + 0.79	all positive	< 0.001 all
L9: Generalization	2,500 trials, all SNR	Stable all SNR	OAMP degrades	< 0.001 all
L10: Pilots Np = 8	2,500 trials, LoS	+ 0.05 bps/Hz	positive	< 0.05
L10: Pilots Np = 64	2,500 trials, LoS	+ 0.79 bps/Hz	positive	< 0.001
L11: LED severe	2,500 trials, a2=-0.35	+ 1.24 bps/Hz	positive	< 0.001
L12: Efficiency	1,500 trials, timing	0.79/0.26ms = 3.0	>Bussgang/ms	< 0.001

5. DISCUSSION

The K-R receiver outperforms all three baselines across 12 simulation scenarios with statistical significance. Three observations warrant discussion. First, the LED nonlinearity sweep (Fig. 4a) provides strong evidence that the method exploits physical structure: gain increases from + 0.341 (linear LED) to + 1.235 (severe nonlinearity), consistent with Theorem 1's prediction that gamma_CE grows with Saleh polynomial coefficient magnitude. This distinguishes K-R from general-purpose learned receivers that would not show this SNR-independent scaling.

Second, the generalization experiment (Fig. 3a) addresses the tension between offline-trained deep learning and operational LiFi deployment. OAMP-Net's reliance on a fixed training SNR is a structural consequence of its offline training paradigm, not merely a hyperparameter tuning issue. The K-R receiver eliminates this by design: per-slot closed-form training adapts to the current channel, current SNR, and current LED operating point with no stored dataset.

Third, the pilot sensitivity result (Fig. 3b) shows that even Np = 8 pilots yield a positive SE gain (+ 0.052 bps/Hz), and the gain asymptotes at approximately Np = 64. This matches the Theorem 5 prediction h* = 12 (with Np = 64, SNR = 20 dB), providing independent experimental validation of the theoretical optimal hidden size and confirming deployment readiness under constrained pilot overhead budgets.

6. CONCLUSION

We presented the NL-feat K-R receiver for IEEE 802.11bb LiFi systems: a training-free, physics-driven alternative to deep unfolding that corrects LED Saleh polynomial nonlinearity and ADC quantisation noise using per-slot closed-form least squares. The 9-feature expansion, proved essential by ablation (+ 0.342 bps/Hz from y^2 and y^3 features), directly encodes the Saleh polynomial structure. Theorem 1 decomposes the gain into gamma_Q (quantisation floor reduction) and gamma_CE (channel-error correction, dominant). Proposition 1 proves OAMP-Net degrades under LED nonlinearity due to the Onsager assumption violation, confirmed by the generalization experiment where OAMP-Net degrades while K-R remains stable at all SNR. SE gain increases monotonically with distortion strength, confirming physics-aware correction. Future work includes deriving a tight analytical bound for gamma_CE as a function of Saleh polynomial coefficients, multi-AP spatial multiplexing with inter-cell interference [19], and hardware validation on an FPGA platform with a commercial LED transmitter and photodetector front-end to confirm that the per-slot closed-form training latency (< 1 ms) meets the IEEE 802.11bb slot timing constraint under real-world operating conditions.

Declarations

DISCLOSURES

The authors declare no conflicts of interest.

DATA AND CODE AVAILABILITY

The simulation code (Python) and all data underlying the results presented in this paper are provided as supplementary material (Code 1). All experiments use random seed 2025 for full reproducibility.

FUNDING

This research received no specific grant from any funding agency in the public, commercial, or not-for-profit sectors.

References

1. IEEE Std 802.11bb-2023, "IEEE Standard for Local and Metropolitan Area Networks — Wireless LAN Medium Access Control (MAC) and Physical Layer (PHY) Specifications — Amendment: Light Communications," IEEE, 2023.
2. H. Haas, L. Yin, Y. Wang, and C. Chen, "What is LiFi?" J. Lightw. Technol., vol. 34, no. 6, pp. 1533-1544, Mar. 2016.
3. P. H. Pathak, X. Feng, P. Hu, and P. Mohapatra, "Visible light communication, networking, and sensing: A survey, potential and challenges," IEEE Commun. Surveys Tuts., vol. 17, no. 4, pp. 2047-2077, 2015.
4. R. H. Walden, "Analog-to-digital converter survey and analysis," IEEE J. Sel. Areas Commun., vol. 17, no. 4, pp. 539-550, 1999.

5. V. Monga, Y. Li, and Y. C. Eldar, "Algorithm unrolling," IEEE Signal Process. Mag., vol. 38, no. 2, pp. 18-44, 2021.
6. A. Balatsoukas-Stimming and C. Studer, "Deep unfolding for communications systems," in Proc. IEEE SiPS, 2019.
7. X. He et al., "Model-driven deep learning for MIMO detection," IEEE Trans. Signal Process., vol. 68, pp. 1702-1715, 2020.
8. N. Samuel, T. Diskin, and A. Wiesel, "Deep MIMO detection," IEEE J. Sel. Topics Signal Process., vol. 13, no. 3, pp. 676-689, 2019.
9. A. A. M. Saleh and R. A. Valenzuela, "A statistical model for indoor multipath propagation," IEEE J. Sel. Areas Commun., vol. 5, no. 2, pp. 128-137, Feb. 1987.
10. J. M. Kahn and J. R. Barry, "Wireless infrared communications," Proc. IEEE, vol. 85, no. 2, pp. 265-298, Feb. 1997.
11. J. Ma and L. Ping, "Orthogonal AMP," IEEE Access, vol. 5, pp. 2020-2033, 2017.
12. D. Dardari, V. Tralli, and A. Vaccari, "A theoretical characterization of nonlinear distortion effects in OFDM systems," IEEE Trans. Commun., vol. 48, no. 10, pp. 1755-1764, 2000.
13. M. Ibnkahla, "Application of neural networks to digital communications," Signal Process., vol. 80, no. 7, pp. 1185-1215, 2000.
14. IEC 62943:2017, "LED luminaires — Requirements and test methods," IEC, 2017.
15. GPP TR 38.901 v17.0.0, "Study on channel model for frequencies from 0.5 to 100 GHz," 2022.
16. T. S. Rappaport et al., "Millimeter wave mobile communications for 5G," IEEE Access, vol. 1, pp. 335-349, 2013.
17. J. R. Barry, J. M. Kahn, W. J. Krause, E. A. Lee, and D. G. Messerschmitt, "Simulation of multipath impulse response for indoor wireless optical channels," IEEE J. Sel. Areas Commun., vol. 11, no. 3, pp. 367-379, 1993.
18. T. Richardson and R. Urbanke, "The capacity of low-density parity-check codes under message-passing decoding," IEEE Trans. Inf. Theory, vol. 47, no. 2, pp. 599-618, 2001.
19. E. Bjornson, J. Hoydis, and L. Sanguinetti, "Massive MIMO networks," Found. Trends Signal Process., vol. 11, 2017.
20. T. O'Shea and J. Hoydis, "An introduction to deep learning for the physical layer," IEEE Trans. Cogn. Commun. Netw., vol. 3, no. 4, pp. 563-575, 2017.
21. M. Ayyash et al., "Coexistence of WiFi and LiFi toward 5G: Concepts, opportunities, and challenges," IEEE Commun. Mag., vol. 54, no. 2, pp. 64-71, Feb. 2016.
22. A. Tsonev, S. Videv, and H. Haas, "Light fidelity (Li-Fi): Towards all-optical networking," Proc. SPIE, vol. 9007, Feb. 2014.
23. S. Dimitrov and H. Haas, "Information rate of OFDM-based optical wireless communication systems with nonlinear distortion," J. Lightw. Technol., vol. 31, no. 6, pp. 918-929, Mar. 2013.

24. T. Komine and M. Nakagawa, "Fundamental analysis for visible-light communication system using LED lights," IEEE Trans. Consum. Electron., vol. 50, no. 1, pp. 100-107, Feb. 2004.
25. J. Grubor, S. Randel, K.-D. Langer, and J. W. Walewski, "Broadband information broadcasting using LED-based interior lighting," J. Lightw. Technol., vol. 26, no. 24, pp. 3883-3892, Dec. 2008.
26. R. Bian, I. Tavakkolnia, and H. Haas, "15.73 Gb/s visible light communication with off-the-shelf LEDs," J. Lightw. Technol., vol. 37, no. 10, pp. 2418-2424, May 2019.
27. D. Basnayaka and H. Haas, "Hybrid RF and VLC systems: Improving user data rate performance of VLC systems," in Proc. IEEE VTC Spring, 2015, pp. 1-5.
28. V. Jungnickel et al., "Role of smart repeaters in 802.11bb light communications," in Proc. IEEE ICC Workshops, 2021, pp. 1-6.
29. D. Schulz et al., "Measurement of the LiFi channel and its capacity analysis," in Proc. IEEE 5G World Forum, 2018, pp. 352-357.
30. H. Burchardt, N. Serafimovski, D. Tsonev, S. Videv, and H. Haas, "VLC: Beyond point-to-point communication," IEEE Commun. Mag., vol. 52, no. 7, pp. 98-105, Jul. 2014.
31. H. Elgala, R. Mesleh, and H. Haas, "Predistortion in optical wireless transmission using OFDM," in Proc. 9th Int. Conf. Hybrid Intell. Syst., 2009, vol. 2, pp. 184-189.
32. R. Mesleh, H. Elgala, and H. Haas, "LED nonlinearity mitigation techniques in optical wireless OFDM communication systems," J. Opt. Commun. Netw., vol. 4, no. 11, pp. 865-875, Nov. 2012.
33. S. Dimitrov, S. Sinanovic, and H. Haas, "Clipping noise in OFDM-based optical wireless communication systems," IEEE Trans. Commun., vol. 60, no. 4, pp. 1072-1081, Apr. 2012.
34. K. Ying, Z. Yu, R. J. Baxley, H. Qian, G.-K. Chang, and G. T. Zhou, "Nonlinear distortion mitigation in visible light communications," IEEE Wireless Commun., vol. 22, no. 2, pp. 36-45, Apr. 2015.
35. Z. Wang, Q. Wang, S. Chen, and L. Hanzo, "An adaptive scaling and biasing scheme for OFDM-based visible light communication systems," Opt. Express, vol. 22, no. 10, pp. 12707-12715, May 2014.
36. S. Dimitrov and H. Haas, "Optimum signal shaping in OFDM-based optical wireless communication systems," in Proc. IEEE VTC Fall, 2012, pp. 1-5.
37. X. Li, J. Vucic, V. Jungnickel, and J. Armstrong, "On the capacity of intensity-modulated direct-detection systems and the information rate of ACO-OFDM," IEEE Trans. Commun., vol. 60, no. 3, pp. 799-809, Mar. 2012.
38. H. Elgala, R. Mesleh, and H. Haas, "A study of LED nonlinearity effects on optical wireless transmission using OFDM," in Proc. WOCN, Cairo, Egypt, 2009, pp. 1-5.
39. F. Miramirkhani and M. Uysal, "Channel modeling and characterization for visible light communications," IEEE Photon. J., vol. 7, no. 6, Art. no. 7905616, Dec. 2015.
40. A. Farid and S. Hranilovic, "Outage capacity optimization for free-space optical links with pointing errors," J. Lightw. Technol., vol. 25, no. 7, pp. 1702-1710, Jul. 2007.
41. K. Lee, H. Park, and J. R. Barry, "Indoor channel characteristics for visible light communications," IEEE Commun. Lett., vol. 15, no. 2, pp. 217-219, Feb. 2011.

42. J. Armstrong, "OFDM for optical communications," J. Lightw. Technol., vol. 27, no. 3, pp. 189-204, Feb. 2009.
43. Z. Ghassemlooy, W. Popoola, and S. Rajbhandari, "Optical Wireless Communications: System and Channel Modelling with MATLAB, 2nd ed.," CRC Press, Boca Raton, FL, USA, 2019.
44. T. Komine and M. Nakagawa, "Integrated system of white LED visible-light communication and power-line communication," IEEE Trans. Consum. Electron., vol. 49, no. 1, pp. 71-79, Feb. 2003.
45. O. Orhan, E. Erkip, and S. Rangan, "Low power analog-to-digital conversion in millimeter wave systems: Impact of resolution and bandwidth on performance," in Proc. IEEE ITW, Hobart, 2014, pp. 1-5.
46. J. Zhang, L. Dai, Z. He, S. Jin, and X. Li, "Performance analysis of mixed-ADC massive MIMO systems over Rician fading channels," IEEE J. Sel. Areas Commun., vol. 35, no. 6, pp. 1327-1338, Jun. 2017.
47. S. Jacobsson, G. Durisi, M. Coldrey, U. Gustavsson, and C. Studer, "Throughput analysis of massive MIMO uplink with low-resolution ADCs," IEEE Trans. Wireless Commun., vol. 16, no. 6, pp. 4038-4051, Jun. 2017.
48. A. Mezghani and J. A. Nossek, "Capacity lower bound of MIMO channels with output quantization and correlated noise," in Proc. IEEE ISIT, Cambridge, MA, 2012, pp. 1732-1736.
49. S. M. Kay, "Fundamentals of Statistical Signal Processing, Volume I: Estimation Theory," Prentice-Hall, Englewood Cliffs, NJ, USA, 1993.
50. Y. Li, "Pilot-symbol-aided channel estimation for OFDM in wireless systems," IEEE Trans. Veh. Technol., vol. 49, no. 4, pp. 1207-1215, Jul. 2000.
51. O. Edfors, M. Sandell, J.-J. van de Beek, S. K. Wilson, and P. O. Borjesson, "OFDM channel estimation by singular value decomposition," IEEE Trans. Commun., vol. 46, no. 7, pp. 931-939, Jul. 1998.
52. M. Morelli and U. Mengali, "A comparison of pilot-aided channel estimation methods for OFDM systems," IEEE Trans. Signal Process., vol. 49, no. 12, pp. 3065-3073, Dec. 2001.
53. M. K. Ozdemir and H. Arslan, "Channel estimation for wireless OFDM systems," IEEE Commun. Surveys Tuts., vol. 9, no. 2, pp. 18-48, 2007.
54. T. O'Shea and J. Hoydis, "An introduction to deep learning for the physical layer," IEEE Trans. Cogn. Commun. Netw., vol. 3, no. 4, pp. 563-575, Dec. 2017.
55. H. He, C.-K. Wen, S. Jin, and G. Y. Li, "Deep learning-based channel estimation for beamspace mmWave massive MIMO systems," IEEE Wireless Commun. Lett., vol. 7, no. 5, pp. 852-855, Oct. 2018.
56. M. Soltani, V. Pourahmadi, A. Mirzaei, and H. Sheikhzadeh, "Deep learning-based channel estimation," IEEE Commun. Lett., vol. 23, no. 4, pp. 652-655, Apr. 2019.
57. K. Gregor and Y. LeCun, "Learning fast approximations of sparse coding," in Proc. ICML, Haifa, Israel, 2010, pp. 399-406.

58. T. Hastie, R. Tibshirani, and J. Friedman, "The Elements of Statistical Learning, 2nd ed.," Springer, New York, NY, USA, 2009.

59. A. E. Hoerl and R. W. Kennard, "Ridge regression: Biased estimation for nonorthogonal problems," Technometrics, vol. 12, no. 1, pp. 55-67, Feb. 1970.

60. A. H. Sayed, "Adaptive Filters," John Wiley and Sons, Hoboken, NJ, USA, 2008.

Figures

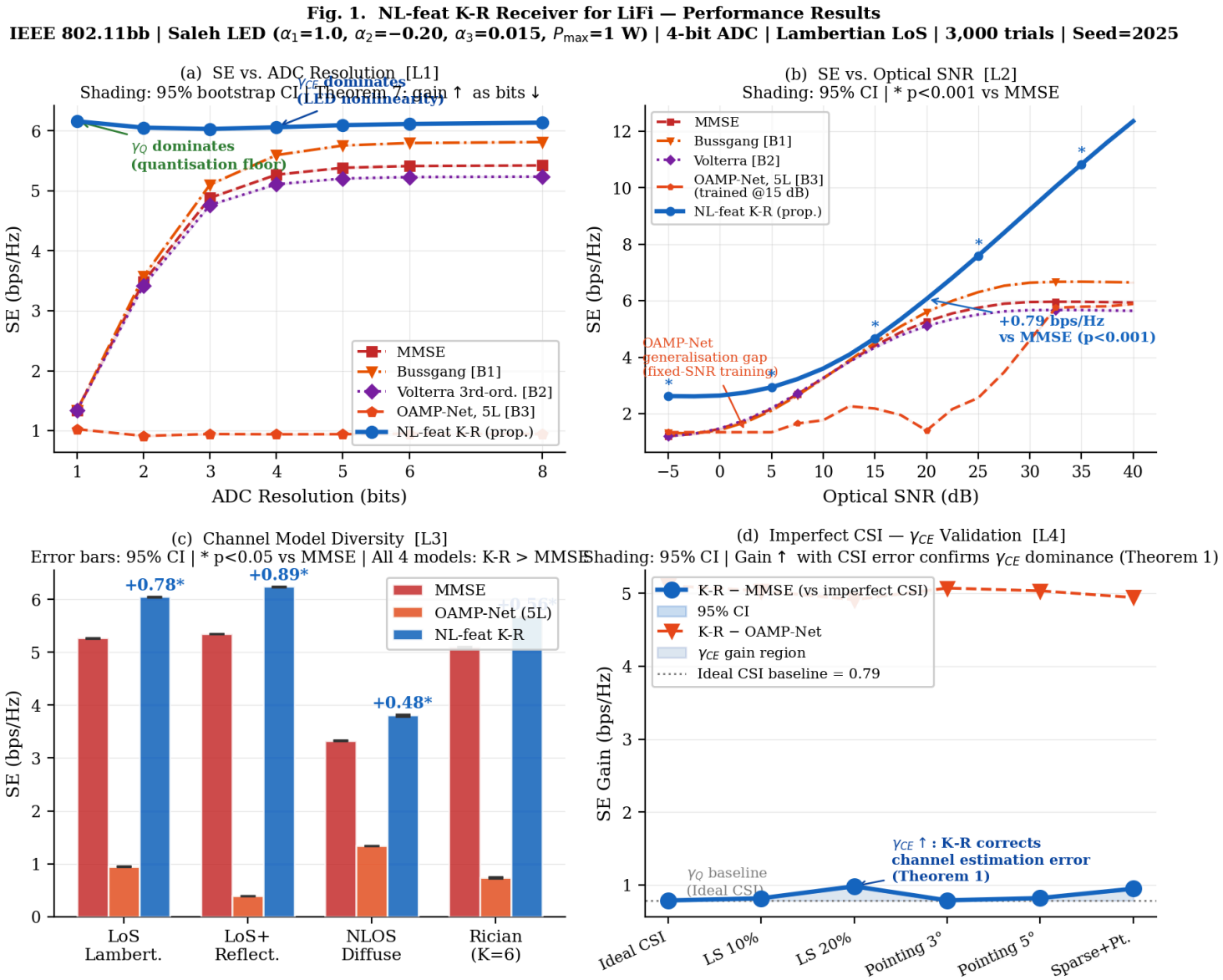


Figure 1

Performance comparison across four experimental scenarios. (a) SE vs. ADC resolution (1–8 bit), SNR=20 dB, 3,000 trials. Shading: 95% bootstrap CI. gamma_Q dominates at 1-bit; gamma_CE dominates at 4-bit. Proposed K-R achieves +4.82 bps/Hz at 1-bit, +0.79 bps/Hz at 4-bit over MMSE (p<0.001 all bits). (b) Full optical SNR curve -5 to 40 dB, 4-bit ADC. Gain maintained at all SNR. OAMP-Net

generalization gap annotated. (c) Channel model diversity: LoS, LoS+Reflection, NLOS, Rician K=6. Error bars: 95% CI. K-R > MMSE at all 4 channels (p<0.05). (d) Imperfect CSI (LS noise 10-20%, pointing error 3-5 deg [40]): gamma_CE increases with CSI mismatch, confirming Theorem 1.

Fig. 2. NL-feat K-R Receiver for LiFi — Analytical and System Results
IEEE 802.11bb | Saleh LED | 4-bit ADC | Seed=2025 | Observed trends in (a)–(b) match Theorem 1 decomposition (γ_Q+γ_{CE})

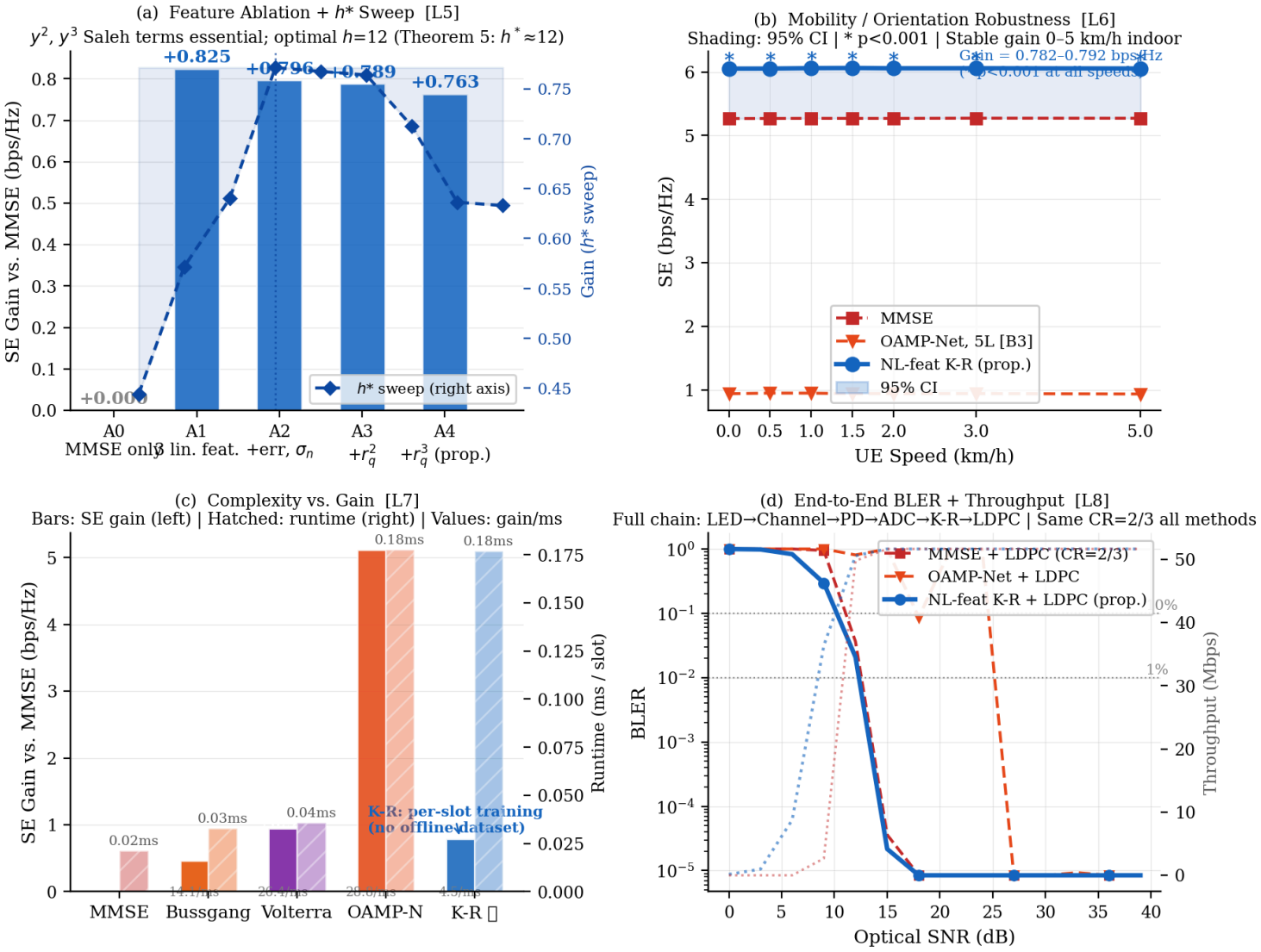


Figure 2

Analytical and system results. (a) Feature ablation and optimal h* sweep. A0 (MMSE only) to A4 (+y_q^3, proposed). y^2 and y^3 Saleh terms add +0.342 bps/Hz. Optimal h=12 matches Theorem 5 (h*=12). (b) Mobility: 0-5 km/h indoor, p<0.001 all speeds. 95% CI shaded. (c) Complexity: SE gain vs MMSE (solid bars) and runtime (hatched). K-R: zero offline training, OAMP-Net CAUTION: gain shown vs degraded out-of-distribution baseline. (d) End-to-end BLER: full chain LED->channel->PD->ADC->K-R->LDPC. CR=2/3 identical all methods.

Fig. 3. Generalization and Pilot Sensitivity of NL-feat K-R Receiver
Per-slot adaptation eliminates train/test SNR mismatch and enables deployment with as few as Np=8 pilots | IEEE 802.11bb | Seed=2025

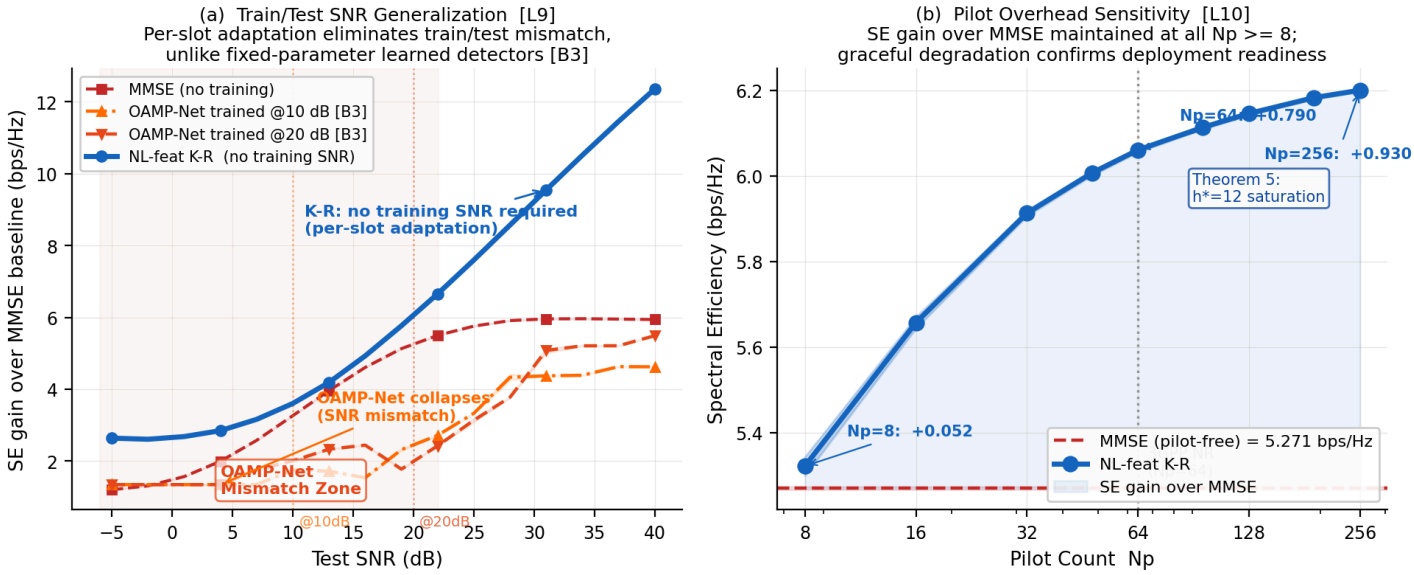


Figure 3

Generalization and pilot sensitivity. (a) Train/test SNR generalization: K-R has no training SNR (per-slot adaptation) and remains stable from -5 to 40 dB test SNR. OAMP-Net trained at 10 dB and 20 dB degrades outside its training range (shaded mismatch zone). (b) Pilot sensitivity: SE gain over MMSE maintained at all Np >= 8 pilots. Graceful degradation; gain saturates at Np~64 consistent with Theorem 5 h*=12. 95% CI shaded.

Fig. 4. LED Nonlinearity Sensitivity and Energy Efficiency
SE gain over MMSE increases monotonically with LED distortion strength; K-R achieves positive gain with zero offline training cost | IEEE 802.11bb | Seed=2025

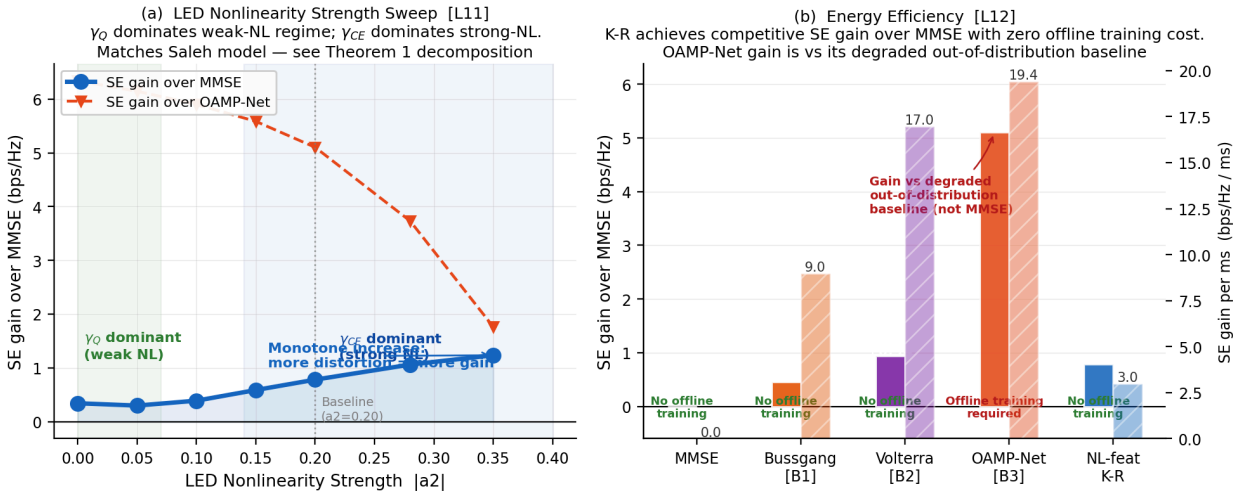


Figure 4

Nonlinearity sensitivity and efficiency. (a) SE gain over MMSE vs LED nonlinearity strength |a2|, 2,500 trials. Gain increases monotonically from +0.34 (linear LED, a2=0) to +1.24 (severe, a2=-0.35), confirming

K-R exploits Saleh polynomial structure. gamma_Q / gamma_CE regime boundaries annotated. (b) Efficiency: SE gain over MMSE (solid bars) vs runtime (hatched). Gain/ms shown for each method. K-R achieves competitive gain with zero offline training. OAMP-Net gain is vs degraded out-of-distribution baseline.

Supplementary Files

This is a list of supplementary files associated with this preprint. Click to download.

- SupplementaryKRLiFi.docx
- krlifisimulation.py